DELTA WINGLETS FOR ENHANCING SOLAR ENERGY: TURBULENT STRAIN RATE-HEAT CONVECTION RELATIONSHIP

Yang Yang,[1] Siddharth Koushik Mohanakrishnan,[1] David S-K. Ting,[1] Steve Ray[2]

ABSTRACT

Delta winglets are an effective means for enhancing heat exchange and thus the performance of renewable energy technologies, including solar energy. A pair of 0.1 mm thick, 15 mm high (h) and 30 mm long aluminum winglets separated with transversal spacing, s, of $2h$, h and 0 were scrutinized in a closed-loop wind tunnel at a Reynolds number based on h of 6300. The turbulent flow was characterized using a 3D hotwire probe, and the heat convection augmentation was quantified in terms of the normalized Nusselt number (Nu/Nu_0), indicating the heat transfer improvement compared to the reference case without the winglets. The interaction of the organized counter-rotational vortices intensifies and they become indiscernible at s = 0. The peak strain rate at 10h downstream increased from 390 s^{-1}, to 478 s^{-1}, to 514 s^{-1}, when the spacing decreased from $2h$ to h to 0, respectively. The zero-spaced winglet pair provided the largest Nu/Nu_0, of around 1.21, at X/h = 10 and Y/h = 0, approximately 21% higher than that of $2h$-spaced winglet pair, due to the strongest strain rate and the absence of upwash flow. On the other hand, the $2h$-spaced winglet pair provided the largest span-averaged Nu/Nu_0, which is of practical significance.

KEYWORDS

delta-winglet pair, turbulent strain rate, heat transfer enhancement

NOMENCLATURE

A	Area of the PTFE (Polytetrafluoroethylene) plate
c	Winglet chord length
E	Uncertainty
H	Convective heat transfer coefficient
h	Winglet height
K_{air}	Thermal conductivity of air
K_{PTFE}	Thermal conductivity of the PTFE plate
L	Characteristic length

1. Turbulence and Energy Laboratory, University of Windsor, ON, Canada
2. Essex Energy, Oldcastle, ON, Canada

N	Sample size
Nu	Nusselt number
Nu_0	Unperturbed reference Nusselt number
PTFE	Polytetrafluoroethylene
$\dot{Q}_{\text{convection}}$	Convective heat transfer rate
$\dot{Q}_{\text{radiation}}$	Radiation heat transfer rate
$\dot{Q}_{\text{total}}$	Total heat transfer rate
s	Transversal space between winglet pair
T_{air}	Ambient air temperature
T_{bottom}	Bottom surface temperature of the *PTFE* plate
T_{top}	Top surface temperature of the *PTFE* plate
T_{wall}	Wall temperature of wind tunnel
t_{PTFE}	Thickness of the *PTFE* plate,
U_i, V_i, W_i	Instantaneous velocity in the X, Y, and Z direction, respectively
$\bar{U}$, $\bar{V}$, $\bar{W}$	Time-averaged velocity in the X, Y, and Z direction, respectively
U_∞	Streamwise freestream velocity
u_i, v_i, w_i	Instantaneous fluctuating velocity in X, Y, and Z direction, respectively
u_{rms}	Streamwise root-mean-square fluctuating velocities
X	Streamwise direction
Y	Widthwise direction
Z	Vertical direction
α	Attack angle of winglet
ε	Emissivity
λ	Taylor microscale
σ	Boltzmann's constant
σ_s	Turbulent strain rate
τ_λ	Taylor time scale

1. INTRODUCTION

To simultaneously improve our environment, health and living standard, much effort has been invested in 'greening' buildings in recent years [1]. Solar energy is, most often, a significant contributor to green buildings. Rock [2] discussed optimizing solar energy collection via building orientation, whereas Alvarado et al. [3] used housing attics. Peng et al. [4] detailed a case study on net-zero-energy solar buildings. Heat exchange is critical in both solar thermal and photovoltaic applications. That being the case, many attempts have been made aiming at improving heat transfer rates. A simple, straightforward, and effective way to improve energy efficiency is to enhance the heat transfer rate passively. Among others, a promising technique is employing winglet-type vortex generators. Winglets can provide long-lasting longitudinal swirling vortices, destabilizing the flow field and disrupting the boundary layer development [5][6], improving

the convective heat transfer and consequently the involved engineering systems. Wu et al. [7] experimentally illustrated the influence of a delta winglet on the heat transfer augmentation of a heated flat plate in an unconfined setting. The winglet was positioned with an attack angle of 30°, 45° and 60° with respect to the incoming flow, which was maintained at 10 m/s, a Reynolds number of 6000 based on the winglet height. According to their study, the winglet with 60° attack angle induced the largest share of the transverse longitudinal vortex and thus, the optimal heat convection enhancement. A numerical investigation of the heat transfer in a circular tube was conducted by da Silva et al. [8]. The attack angle of the winglet was varied from 15° to 45°, for a Reynolds number based on the diameter of the circular channel ranging from 300 to 900. Over the range of studied conditions, increasing the attack angle augmented the heat transfer rate. The Nusselt number was enhanced by around 40%, when the attack angle was 15° and the Reynolds number was 900, compared to the reference case without the winglet. This heat transfer augmentation increased to 68% at an attack angle of 45°.

Instead of a single winglet, winglet pairs or arrays are more appropriate when it comes to a large heat transfer surface such as a relatively large heat exchanger tube or a photovoltaic panel or array. Sun et al. [9] experimentally examined the effect of the number of winglets on the heat transfer in a circular tube. They showed that the heat transfer rate in terms of Nusselt number increased with the number of winglets, due to the added fluid mixing across the tube. Li et al. [10] carried out a numerical study, investigating the arrangement of a pair of delta winglets for heat transfer augmentation in a half coiled jacket pipe. They concluded that the common-flow-up (CFU) configuration of the winglet pair could provide a stronger secondary flow motion and thus, better thermal transportation compared to the common-flow-down (CFD) configuration. The CFU winglet pair resulted in an approximately 16% increase in the average Nusselt number, whereas the CFD configuration led to a 9% increase. The effect of the shape of winglet pair on heat convection of a fin-tube heat exchanger was numerically investigated by Hu et al. [11]. They pointed out that the intensity of the vortex plays a significant role in heat transfer augmentation. Therefore, the delta winglet pair, from which the largest vortex intensity was observed, provided the best heat transfer augmentation, compared to the rectangular and trapezoidal winglet pairs. In another study, the delta winglet pair and rectangular winglet pair were proposed for the heat transfer enhancement in a double-pipe heat exchanger by Li et al. [12]. They found that a better heat transfer augmentation was achieved when the delta winglet pair was utilized, with Nusselt number increased by 71% to 78% at a Reynolds number from 6600 to 13400. The Nusselt number enhancement of the rectangular winglet pair was around 52%-67% at the same Reynolds conditions. Zhai et al. [13] developed an experimental investigation, optimizing the attack angle (10° to 40°), height (5 mm, 7.5 mm, 10 mm) and spacing (10 mm, 15 mm, 20 mm) of the delta winglet pair to maximize the heat transfer enhancement in a circular tube. The Reynolds number in this study ranged from 5000 to 25000. It was found that the heat convection, in terms of Nusselt number, increased with Reynolds number regardless of the attack angle, height and spacing of the winglet pair. Further, they concluded that the winglet pair with the largest attack angle (40°), tallest height (10 mm) and middle spacing (15 mm) provided the highest heat transfer enhancement, with a maximum normalized Nusselt number of around 1.73.

It is interesting to note from the aforementioned studies that the heat convection augmentation could be considerably improved by an appropriately designed winglet pair. The design parameters include the arrangement, shape, attack angle, height, transversal space, etc., as summarized in Table 1. Among others, the spacing effect on the heat transfer seems more

ambiguous. The optimal heat transfer does not necessarily occur with the narrowest nor the widest spacing. For example, in Ref [13], the best heat transfer was obtained with a moderately-spaced winglet pair. Pourhedayat et al. [14] numerically explored the effect of winglet pair spacing on the heat transfer in a circular tube. The pair of winglets in this study were separated by 0 to 40 mm, and the diameter of the tube was 47 mm. In their study, the 20 mm-spaced winglet pair provided the maximum heat transfer augmentation. In another study conducted by Song et al. [15][16], a pair of winglets separated by 0, 0.6, 1, 1.3 $L\sin\theta$ were investigated, where L and θ were the winglet base length and attack angle, respectively. This study showed that the winglet pair with the second smallest space (0.6 $L\sin\theta$) provided the best heat transfer enhancement in the fin-tube heat exchanger.

From the fundamental perspective, flow destabilization is one of the promising mechanisms for passive heat transfer enhancement [5]. An increase in fluctuating velocity can result in a significant increase in heat transfer enhancement [17][18]. In addition to flow fluctuations, the turbulent length scales are also of significance to better describe the turbulent flow, which is rich in eddying motions of different sizes [19]. Therefore, the turbulent strain rate, incorporating both the effect of turbulent fluctuating intensity and that of length scale, comes to mind.

TABLE 1. Summary of previous studies about the effect of winglet on heat transfer enhancement.

Reference	Condition	Studied parameters	Main finding
Wu et al. [7]	Open flow	Attack angle: 30° to 60°	Heat transfer rate increases with attack angle
da Silva et al. [8]	Channel flow	Attack angle: 15° to 45°	Heat transfer rate increases with attack angle
Sun et al. [9]	Channel flow	Number of winglets: 4, 6, 8	Heat transfer rate increases with number of winglets
Li et al. [10]	Channel flow	Configuration: common-flow-up and common-flow-down	Common-flow-up provided a better heat transfer performance
Hu et al. [11]	Channel flow	Shape: delta, rectangular, trapezoidal winglet	Delta winglet provided the best heat transfer performance
Li et al. [12]	Channel flow	Shape: delta, rectangular winglet	Delta winglet provided a better heat transfer performance
Zhai et al. [13]	Channel flow	Attack angle: 10° to 40°; height: 5 mm, 7.5 mm, 10 mm; spacing: 10 mm, 15 mm, 20 mm	Heat transfer rate increases with the increase of attack angle and height; 15 mm-spaced winglet pair provided the largest heat transfer enhancement
Pourhedayat et al. [14]	Channel flow	Spacing: 0 to 40 mm	20 mm-spaced winglet pair provided the laregest heat transfer augmentation
Song et al. [15][16]	Channel flow	Spacing: 0, 0.6, 1, 1.3 $L\sin\theta$, L and θ were the winglet base length and attack angle	0.6 $L\sin\theta$ provided the largest heat transfer enhancement

TABLE 2. Highlighted contributions of the current study.

• The less-known spacing effect of a winglet pair is investigated.
• Different from most previous studies conducted within the confinement of a channel, the current study is carried out in open flow condition.
• The correlation between turbulent strain rate and heat transfer enhancement is deduced.

So far, notable investigations have been developed in characterizing a turbulent flame in terms of the turbulent strain rate [20][21]. However, its effect on convective heat transfer is relatively unexplored. With this backdrop, the current study aims at scrutinizing the spacing effect of a winglet pair on the turbulent strain rate and the heat transfer enhancement over a heated flat plate. The highlighted contributions are summarized in Table 2. With this understanding, engineers can better design winglets for potent heat transfer enhancement.

2. EXPERIMENTATION

This experimental investigation was carried out in a closed-loop wind tunnel with a 760 mm square cross-section. The detailed setup, including the studied delta winglet pair, is depicted in Figure 1. A PTFE (polytetrafluoroethylene) plate was inlaid in the base of the test section. It is 295 mm wide, 380 mm long, and 3 mm thick, with a thermal conductivity and emissivity of $0.25 \mathrm{Wm^{-1}K^{-1}}$ [22] and 0.92 [23], respectively. Under the PTFE plate, a tank of water was heated to boil continuously, with the generated steam condensing on the lower surface. As a consequence, a uniform temperature of approximately 100°C was maintained on the bottom surface of the PTFE plate. In this study, a FLIR C2 thermal camera was employed to obtain the top surface temperature distribution of the PTFE plate, and thus, the heat transfer augmentation, in terms of the normalized Nusselt number could be deduced. The 0.1 mm thick

FIGURE 1. Experimental setup.

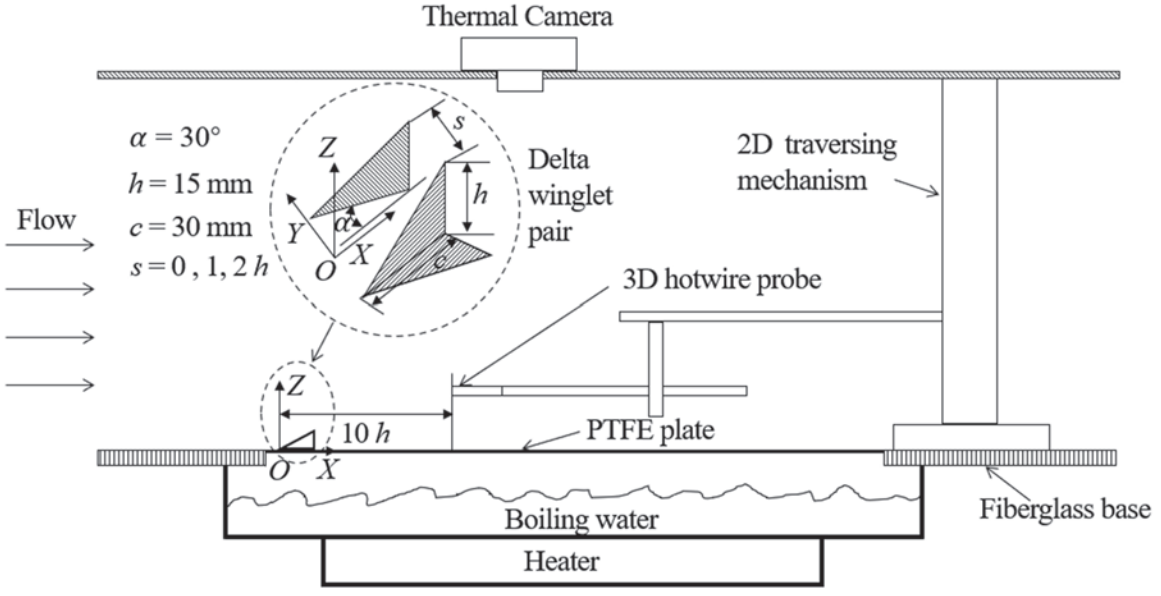

aluminum winglets have height (h) of 15 mm and chord length (c) of 30 mm. They were placed side-by-side in a common-flow-up configuration [10] on the PTFE plate. The transversal space (s) of the trailing edge of the winglet pair was $2h$, h and 0. The attack angle (α) of the winglets was maintained at 30°. The origin O was chosen as the middle point between the tips of the winglet pair, and the orthogonal X, Y, and Z representing the streamwise, widthwise and vertical direction, respectively. The incoming flow in this study was set at 7 m/s, the corresponding Reynolds number was approximately 6300 based on the winglet height. To characterize the turbulent strain rate behind the winglet pair, a 3D hotwire probe with a constant-temperature anemometer (type 55P95) was utilized to quantify the flow at $10h$ downstream from the leading edge of the winglet pair. The cross-stream measure plane was $8h$ by $2.67h$, with spatial resolution of $0.33h$. At each measure point, the velocity signal was low-passed at 30 kHz and sampled at 80 kHz, with sampling number of 10^6 to avoid aliasing.

3. DATA PROCESSING

With a 3D hotwire probe, the instantaneous velocities in all three orthogonal directions could be obtained. The streamwise, widthwise and the vertical velocities can be expressed as,

$$U_i = \bar{U} + u_i; \quad V_i = \bar{V} + v_i; \quad W_i = \bar{W} + w_i \tag{1}$$

where $\bar{U} = \frac{1}{N}\sum_{i=1}^{N} U_i$, $\bar{V} = \frac{1}{N}\sum_{i=1}^{N} V_i$, $\bar{W} = \frac{1}{N}\sum_{i=1}^{N} W_i$ are the time-averaged velocities, and u_i, v_i, and w_i are the corresponding fluctuating velocity, from which the root-mean-square turbulent fluctuating velocity could be calculated,

$$u_{\text{rms}} = \sqrt{\sum_{i=1}^{N} \frac{u_i^2}{N-1}} \tag{2}$$

Here, N is the sampling size, which is set at one million in this study. Also, from the fluctuating velocity, the Taylor timescale could be obtained, i.e.,

$$\tau_\lambda = \sqrt{\frac{\overline{2u^2(t)}}{\left[\frac{du(t)}{dt}\right]^2}} \tag{3}$$

Invoking the Taylor frozen hypothesis [24], the Taylor microscale can be deduced by multiplying the Taylor timescale with the velocity conveying the eddies across the hotwire. Specifically, the Taylor microscale,

$$\lambda = \bar{U}\tau_\lambda \tag{4}$$

Instead of relating the heat transfer with a characteristic turbulent velocity and a suitable length scale separately, an appropriate turbulent parameter incorporating both velocity and length scales can be devised. Turbulent strain rate is such a parameter signifying the flow straining caused by the intense vortex tubes represented by the Taylor microscale. This turbulent strain rate can be expressed as

$$\sigma_s = \frac{u_{\text{rms}}}{\lambda} \tag{5}$$

With negligible conduction heat transfer, the convective heat transfer rate of the studied heated PTFE plate could be expressed as the total heat transfer rate minus radiation heat transfer rate, i.e.,

$$\dot{Q}_{\text{convection}} = \dot{Q}_{\text{total}} - \dot{Q}_{\text{radiation}} \tag{6}$$

where the total heat could be obtained from,

$$\dot{Q}_{\text{total}} = K_{\text{PTFE}} A \left(\frac{T_{\text{bottom}} - T_{\text{top}}}{t_{\text{PTFE}}} \right) \tag{7}$$

Here, K_{PTFE} is equal to 0.25 $\text{Wm}^{-1}\text{K}^{-1}$ [22], which is the thermal conductivity of the PTFE plate. The thickness and the area of the PTFE plate, t_{PTFE} and A are 3 mm and 295 mm by 380 mm, respectively. T_{top} is the top surface temperature of the heated plate, which is measured by the thermal camera, and T_{bottom} is bottom surface temperature, which is maintained at 100°C.

The radiation heat transfer rate,

$$\dot{Q}_{\text{radiation}} = \varepsilon \sigma A \left(T_{\text{top}}^4 - T_{\text{wall}}^4 \right) \tag{8}$$

where emissivity ε is 0.92 [23], and the Stefan-Boltzmann constant σ is 5.67×10^{-8} $\text{Wm}^{-2}\text{K}^{-4}$ [25]. T_{wall} is the wall temperature of the wind tunnel, which is around 23°C.

The convective heat transfer coefficient could be deduced from $\dot{Q}_{\text{convection}}$,

$$H = \frac{\dot{Q}_{\text{convection}}}{A\left(T_{\text{top}} - T_{\text{air}} \right)} \tag{9}$$

where the air temperature, T_{air}, is 23°C. This convective heat transfer coefficient could be normalized by the thermal conductivity of the ambient air (K_{air}) and the characteristic length (L), giving the Nusselt number,

$$Nu = \frac{HL}{K_{\text{air}}} \tag{10}$$

As we are interested in the heat transfer augmentation and not the heat transfer rate itself, the Nusselt number is normalized by the corresponding reference Nusselt number in the absence of the winglet pair (Nu_0),

$$\frac{Nu}{Nu_0} = \frac{H}{H_0} \tag{11}$$

4. RESULTS AND DISCUSSION

4.1 Flow and turbulent strain rate

Random fluctuation is one of the basic characteristics of the turbulent flow [19]. Therefore, the streamwise root-mean-square fluctuating velocity (u_{rms}) at X/h = 10 is shown in Figure 2. The uncertainty, presented in the Appendix, is around 0.02 ms^{-1}. The cross-sectional velocity vectors are also presented in the figures to show the flow field. The two dashed-line triangles trace the winglets in the *YZ* plane, looking upstream at 10*h* downstream. When the transversal space, *s*, between the two winglets is 2*h*, a pair of counter-rotational swirling flows could be clearly seen; see Figure 2(a). These organized flow structures cause a notable flow motion, upwash, vertically upward away from the heated surface, locating at around Y/h = 0. This could have a negative effect on the heat transfer enhancement [7], because the upwash leaves behind a quasi-stagnant region next to the surface. With decreasing spacing between the winglets, the

FIGURE 2. Streamwise root-mean-square fluctuating velocity (ms^{-1}) and velocity vector in *YZ* plane at 10h downstream of the winglet pair separated by (a) 2*h* (b) 1*h* (c) 0.

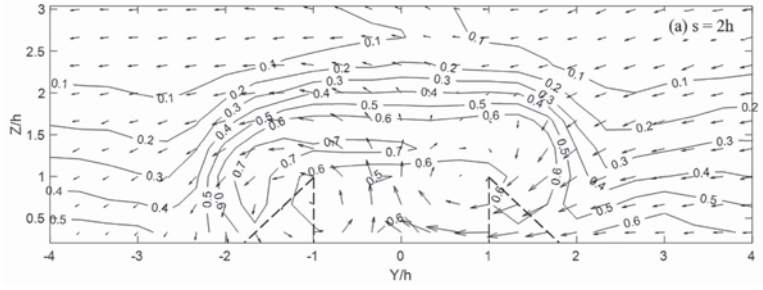

(a)

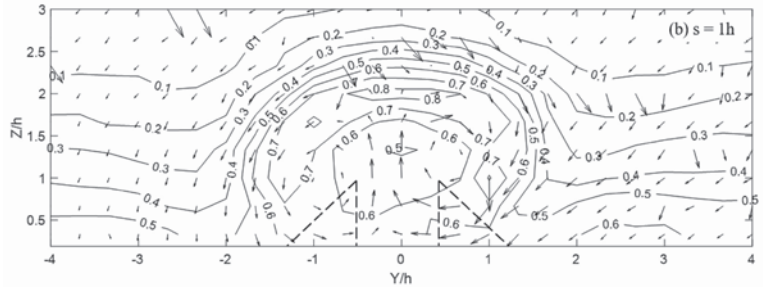

(b)

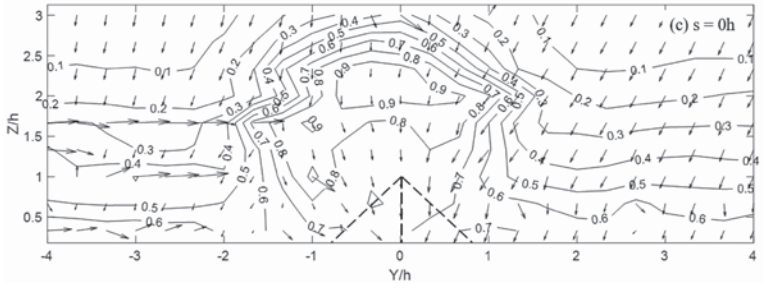

(c)

TABLE 3. Peak value of u_{rms}

Spacing between winglets	Maximum u_{rms}
$s = 2h$	0.75 ms^{-1}
$s = 1h$	0.86 ms^{-1}
$s = 0$	0.97 ms^{-1}

interaction of the large, organized vortices becomes stronger. This interaction is most intense when the two winglets touch each other, with $s = 0$, in which case the two organized vortices become literally indistinguishable; see Figure 2(c). Due to the finite resolution of the measurement locations, they appear to merge into one vortex, which is not the case. More importantly, the intensification of vortex-vortex interaction leads to intensification of the turbulence fluctuation. From Figure 2(a), we can see that u_{rms} peaks at around 0.75 ms^{-1}, at $Y/h = -1.67$, $Z/h = 0.67$. This corresponds to the core of the swirling vortex [26]. With decreasing separation between the two winglets, s, the intense u_{rms} region tends to move toward the center, i.e., $Y/h = 0$, where the two vortices strongly interact with each other. Also, the peak u_{rms} increases to around 0.86 ms^{-1} and 0.97 ms^{-1}, when the spacing of the winglet pair decreases to $1h$ and 0, respectively; see Table 3. Besides, a decreasing trend of turbulence fluctuation with respect to the vertical direction, Z/h, is also identified. This indicates that the turbulence fluctuation is also associated with the boundary layer, and it is being restored to the unperturbed condition as the freestream is approached.

Figure 3 illustrates the contour of Taylor microscale (λ), which represents the small dissipative turbulent length scale. The uncertainty of the Taylor microscale is estimated to be around 0.10 mm; see Appendix. Note that a couple of considerably small values tend to appear far away from the wake of winglet pair, where the flow is largely laminar and the turbulent length scale is meaningless. Thus, we only focus on the wake region of the winglet, where the turbulence fluctuation is of significance. Corroborating with the general decreasing trend of turbulence fluctuation shown in Figure 2, an increase of Taylor microscale with respect to Z/h could be clearly observed. For the $2h$-spaced winglet pair, the minimum value of Taylor microscale is around 1.4 mm, located near the wall surface at $Y/h = -0.33$, $Z/h = 0.67$. With increasing Z/h, λ increases rapidly and reaches a maximum value of around 4.5 mm at $Y/h = 0$ and $Z/h = 1.67$; see Figure 3(a) and Table 4. When it comes to the 1h-spaced winglet pair shown in Figure 3(b), the minimum λ is around 1.4 mm, the same level with that of $2h$-spaced winglet pair. Meanwhile, the increase of the Taylor microscale with Z/h seems more gradual, with a smaller λ peak of around 3.9 mm at $Y/h = 0$ and $Z/h = 2$. When the separation between the two winglets is reduced to 0, the Taylor microscale becomes smaller than 3 mm near $Y/h = 0$; see Figure 3(c). This is presumably caused by the strongest vortex-vortex interaction and the most intense turbulence fluctuation as shown in Figure 2(c).

Figure 4 depicts the contour of turbulent strain rate over a cross section at $10h$ downstream from the leading edge of the winglet pairs with varying spacing. Generally, the decreasing space results in an increase of turbulent straining. It is clear from Figure 4(a) that for $s = 2h$, the turbulent strain rate reaches a peak value of around 390 s^{-1}, near $Y/h = 0$, $Z/h = 0.33$. The uncertainty of the strain rate is estimated to be approximately 23 s^{-1}, see the Appendix. The location of the maximum strain rate region corresponds to the vortex interaction area and the

FIGURE 3. Streamwise Taylor microscale (mm) and velocity vector in *YZ* plane at 10*h* downstream of the winglet pair separated by (a) 2*h* (b) 1*h* (c) 0.

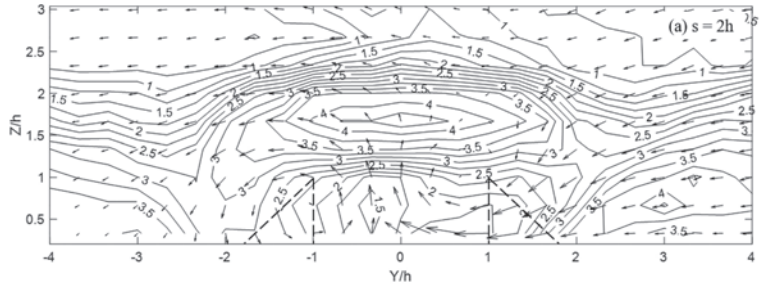

(a)

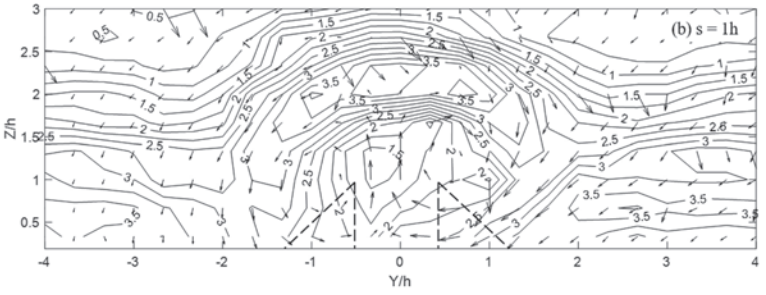

(b)

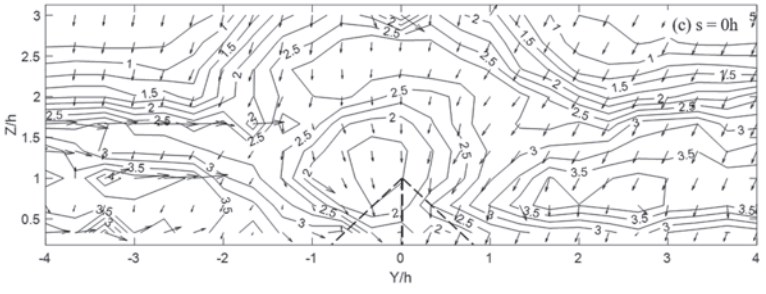

(c)

TABLE 4. Largest λ near $Y/h = 0$.

Spacing between winglets	Largest λ
$s = 2h$	4.5 mm
$s = 1h$	3.9 mm
$s = 0$	3 mm

near-wall boundary, where the turbulence fluctuation is large and the Taylor microscale is small. When decreasing the transversal spacing to 1*h* and 0, the peak values of the turbulent straining increased to around 478 s^{-1} and 514 s^{-1}, respectively; see Table 5. This is expected to have a positive effect on the heat transfer near $Y/h = 0$, which will be discussed in the following section.

FIGURE 4. Turbulence strain rate contour (s^{-1}) and velocity vector in *YZ* plane at 10*h* downstream of the winglet pair separated by (a) 2*h* (b) 1*h* (c) 0.

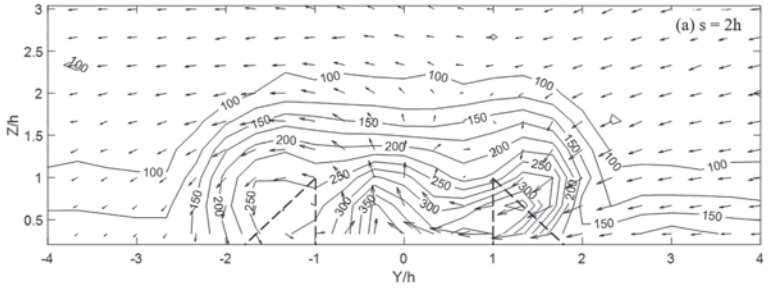

(a)

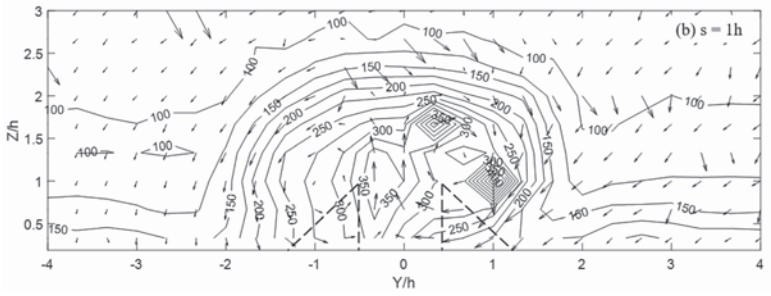

(b)

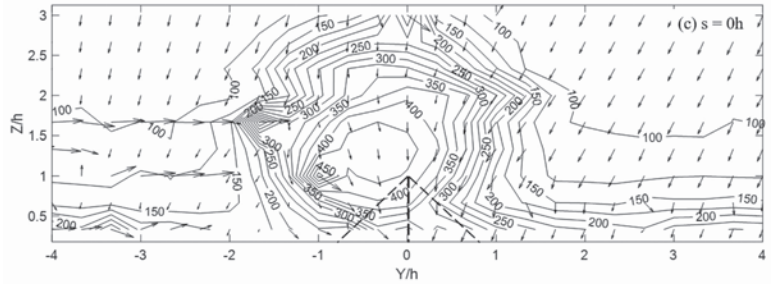

(c)

TABLE 5. Maximum turbulent strain rate.

Spacing between winglets	Maximum turbulent strain rate
$s = 2h$	390 s^{-1}
$s = 1h$	478 s^{-1}
$s = 0$	514 s^{-1}

4.2 Heat transfer

To scrutinize the heat convection enhancement compared to the reference case in the absence of a winglet pair, the normalized Nusselt number (Nu/Nu_0) is illustrated in Figure 5. The uncertainty of Nu/Nu_0 is around 0.066, see the Appendix. The origin point (X/h = 0, Y/h = 0) corresponds to the middle point between the tips of the winglet pair. The black triangles are the attached fold of the pair of aluminum winglets; they are highly conductive and hence promoted heat loss in the proximity. From Figure 5(a), two convection-enhanced areas could be clearly found, span across from Y/h = ±0.5 to ±3. These correspond to the locations of the

FIGURE 5. Normalized Nusselt number (Nu/Nu_0) downstream of the winglet pairs.

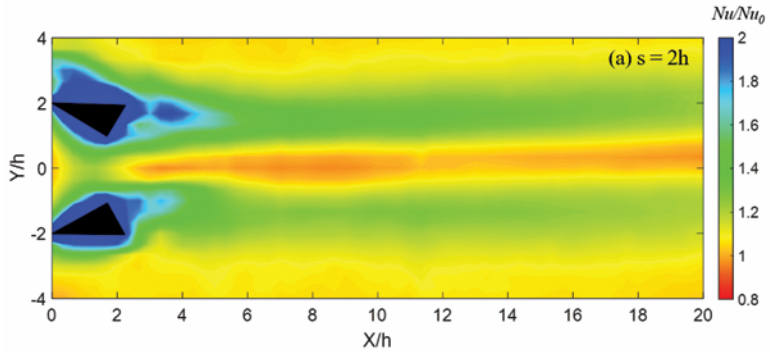

(a)

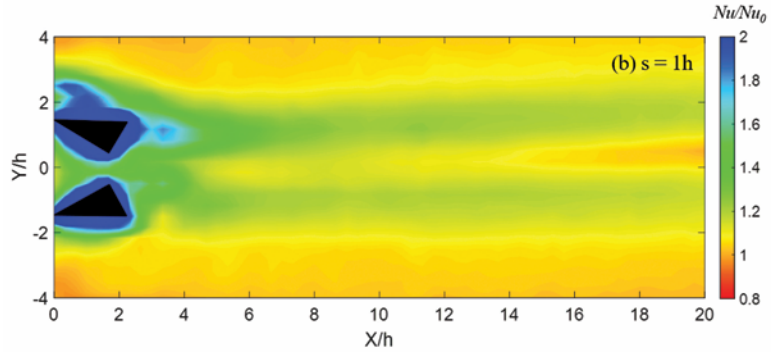

(b)

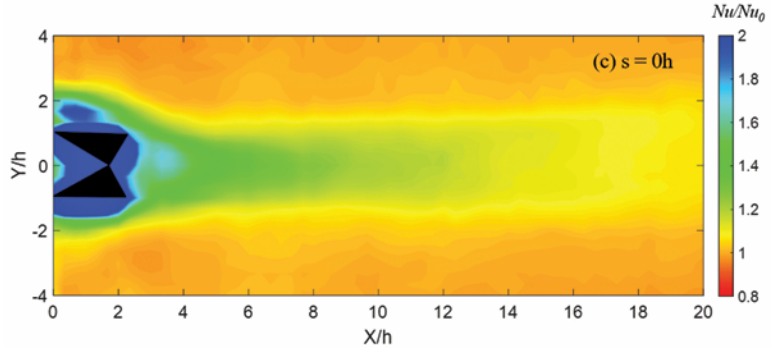

(c)

TABLE 6. Maximum normalized Nusselt number (Nu/Nu_0) at the end of studied surface.

Spacing between winglets	Location	Nu/Nu_0
$s = 2h$	$X/h = 20$, and $Y/h = -1.33$	1.21
$s = 1h$	$X/h = 20$, and $Y/h = -0.83$	1.16
$s = 0$	$X/h = 20$, and $Y/h = 0$	1.08

counter-rotational vortices as shown in Figure 2(a). Nu/Nu_0 decreases gradually with respect to the downstream direction, implying the weakening of the vortical flow with streamwise distance. Nevertheless, the convective heat transfer is still enhanced by around 20% at X/h = 20, and $Y/h = -1.33$, the end of the studied area. This indicates the long-lasting effect resulting from the longitudinal vortices created by the winglet pair. Also, worth mentioning is that, at the area near $Y/h = 0$, the heat transfer enhancement is considerably weak; see Figure 5(a). In spite of the more intense turbulent straining motion, the upwash flow was also observed in this region as shown in Figure 4(a), which tends to reduce heat convection [27]. With decreasing separation between the winglets, the two side-by-side convection-enhanced areas start to merge with each other. When the spacing is zero, only one enhanced area near $Y/h = 0$, where the most intense strain rate resides, is seen; see Figures 4(c) and 5(c). Without a clear upwash flow region for the zero-spaced winglet pair, the effect of turbulent strain rate on heat convection is expected to prevail. The correlation between the strain rate and heat transfer will be discussed later. Meanwhile, from Figure 5(c), a smaller Nu/Nu_0 is observed near the end of the heated surface, of around 1.08 at $X/h = 20$, and $Y/h = 0$, also shown in Table 6. This is probably due to the absence of the pair of organized swirling vortex streets, an outcome of the intense vortex-vortex interaction in the near wake which somewhat disintegrated the two vortex streets.

To take a closer look at heat convection augmentation, the cross-stream normalized Nusselt number (Nu/Nu_0) at $X/h = 10$ is depicted in Figure 6. Clearly, the convective heat transfer enhancement peaks at around $Y/h = \pm 2$ for $2h$-spaced winglet pair, corresponding to the downwash flow regions, where the freestream cooler air is more effectively transported toward the heated surface; see Figure 2(a). Also, a valley of Nu/Nu_0 is observed at $Y/h = 0$, where the upwash flow locates. With the transversal space of the winglet pair decreases from $2h$ to h, the valley Nu/Nu_0 near $Y/h = 0$ increases from 1.0 to around 1.12. This is partially due to the increase of the turbulent strain rate. Meanwhile, the peak value decreases from around 1.35 to 1.23. Decreasing the separation further, from h to zero, the peak value decreases to around 1.21. This peak, instead of the minimum, Nu/Nu_0 occurs at $Y/h = 0$. In summary, the decrease in the transversal spacing tends to increase the minimum value while decreasing the peak value.

Figure 7 shows the span-averaged normalized Nusselt number (Nu/Nu_0) with respect to the downstream distance, which is of practical significance, as the heat transfer of the entire surface is taken into consideration. Recall that potential winglet applications include the cooling of solar photovoltaic panels and enhancing solar air heaters [28]. The values plotted in Figure 7 are Nu/Nu_0 averaged across $Y/h = \pm 4$, the whole span area shown in Figure 5. The plot starts at X/h of 3, omitting the area affected by the conductive aluminum winglets acting as heat fins. From the figure, we can see that the largest Nu/Nu_0 occurs right behind the winglet, due to the strongest vortices with the most intense turbulence. The span-averaged Nu/Nu_0 for the $2h$-spaced winglet

FIGURE 6. Cross-stream normalized Nusselt number (Nu/Nu_0) at X/h = 10.

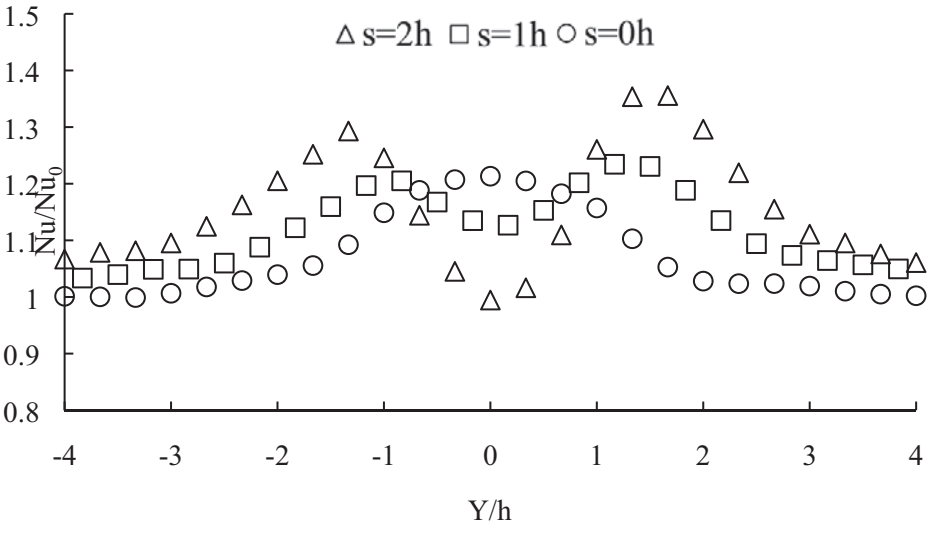

FIGURE 7. Span-averaged normalized Nusselt number (Nu/Nu_0) downstream of the winglet pairs (span-averaged across $Y/h = \pm 4$).

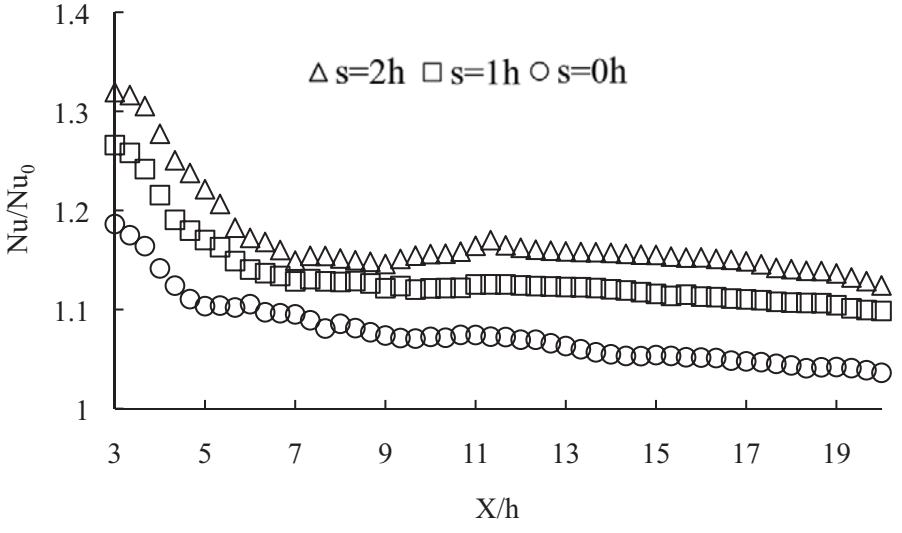

pair is around 1.32 at X/h = 3. It decreases rapidly to 1.17 with streamwise distance up to X/h of 6, beyond which the decrease is more gradual. Nu/Nu_0 reaches a value of around 1.12 at the end of the studied span at X/h = 20. With decreasing transversal spacing between the pair of the winglets, the averaged heat transfer augmentation tends to decrease. For the zero-spaced winglet pair, the span-averaged Nu/Nu_0 at X/h = 3 and 20 are approximately 1.19 and 1.04, around 0.13 and 0.08 smaller than those associated with the 2h-spaced winglet pair.

Figure 8 presents the correlation between the normalized Nusselt number and the turbulent strain rate. Note that the strain rate values here are the vertical averaged values from Z/h = 0.33 to 3 in Figure 4. From Figure 8(a), we can see that the correlation between Nu/Nu_0 and strain rate is weak. The increase of strain rate tends to increase the heat transfer augmentation.

FIGURE 8. Correlation between normalized Nusselt number and vertical-averaged strain rate.

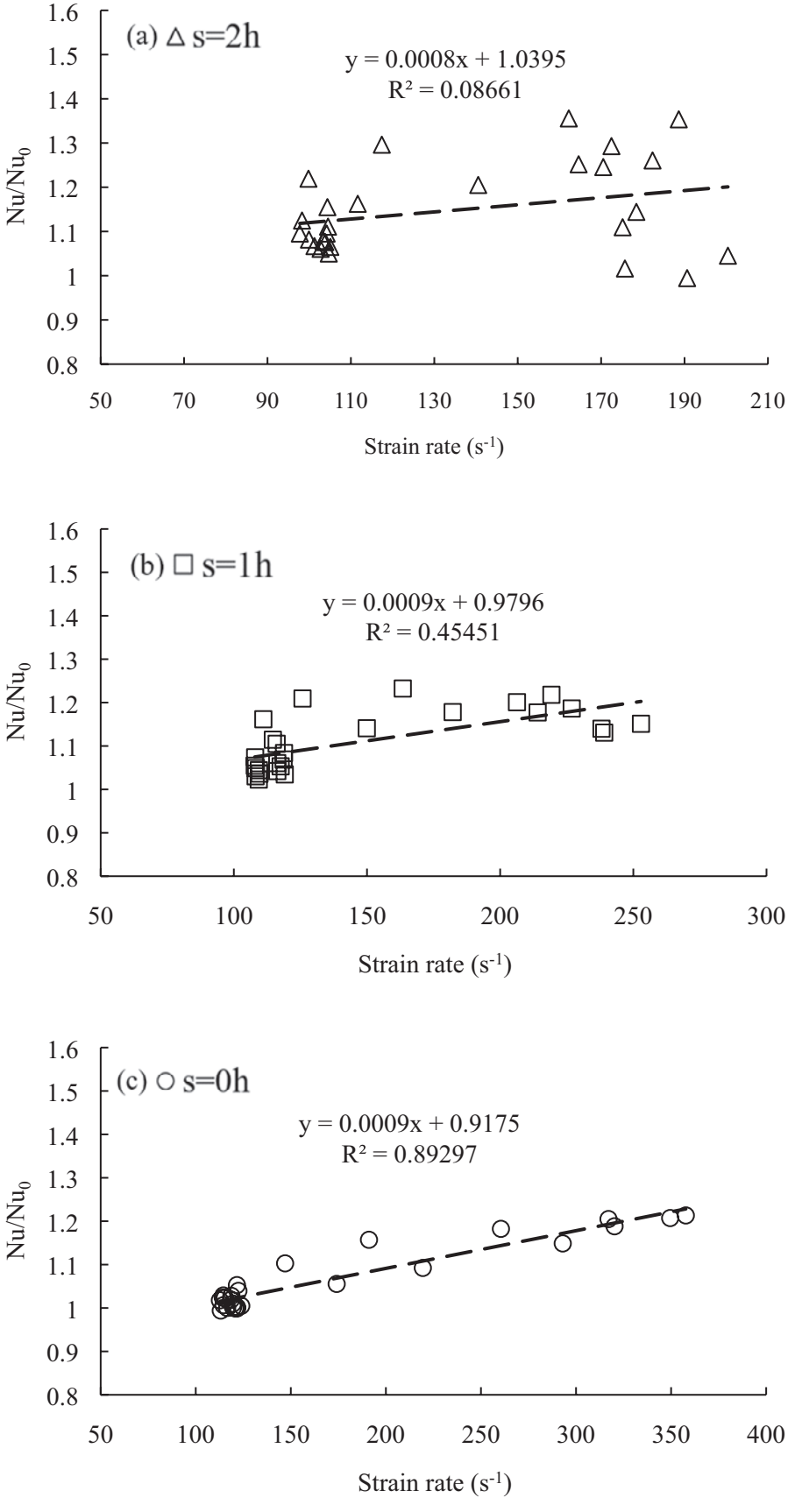

However, a couple of points at the high strain rate end deviate quite significantly from the increasing trend, i.e., the strain rate is large, but the corresponding Nu/Nu_0 is small. These values are located near $Y/h = 0$, where the upwash flow appears. In other words, the upwash flow seems to offset the positive effect of the turbulent straining, resulting in a reduction of Nu/Nu_0. With decreasing transversal spacing between the winglets, the correlation between Nu/Nu_0 and strain rate becomes stronger. When it comes to the zero-spaced winglet pair, an approximately linear increasing trend could be clearly observed; see Figure 8(c). This indicates that, due to the strong interaction and the destruction of the organized vortices, the turbulent strain rate, incorporating both turbulent fluctuation and length scale, becomes the dominant factor dictating the extent of convection heat transfer enhancement.

5. CONCLUSIONS

A pair of 15 mm high (h), 30 mm long delta winglets were experimentally explored for their effectiveness in generating turbulent strain rate and hence augmenting the heat convection from a heated flat surface. The pair of winglets was separated by $2h$, h and 0 in 7 m/s wind. The main findings are summarized as follows.

1. The stronger the vortex-vortex interaction, the more intense the resulting turbulent strain rate. With decreasing transversal spacing from $2h$ to h to 0, the peak of turbulent strain rate increases from 390 s^{-1} to 478 s^{-1} to 514 s^{-1}, respectively.
2. Due to the strongest vortex-vortex interaction, the zero-spaced winglet pair led to the highest Nu/Nu_0 value around the middle region, i.e., $Y/h = 0$. The peak Nu/Nu_0 is approximately 1.21 at $X/h = 10$, $Y/h = 0$, roughly 0.21 larger than that associated with the $2h$-spaced winglet pair. However, the $2h$-spaced winglet pair provided the largest span-averaged Nu/Nu_0 value from the beginning to the end of the studied heated surface. This indicates that the $2h$-spaced winglet pair is more effective in enhancing heat convection over the span of the studied flat surface. This is of practical significance as few winglets are needed to promote heat transfer over a long stretch of surface.
3. The local turbulent strain rate correlates well with the local heat transfer enhancement, Nu/Nu_0. An approximately linear correlation between strain rate and heat convection enhancement was identified in the absence of the organized swirling vortex structure for the case of the zero-spaced winglet pair.

ACKNOWLEDGMENTS

This work was made possible by Natural Sciences and Engineering Research Council of Canada and Ontario Centres of Excellence.

REFERENCES

[1] "Green Building—US Environmental Protection Agency." [Online]. Available: https://archive.epa.gov/green-building/web/html/. [Accessed: 08-Sep-2020].
[2] B. A. Rock, "Comparing building surfaces' orientations to optimize solar energy collection," *J. Green Build.*, vol. 15, no. 2, pp. 3–28, 2020, doi: 10.3992/1943-4618.15.2.3.
[3] R. G. Alvarado;, P. G. Campos;, and P. Wegertseder, "Optimal design of housing attics with integrated solar collectors," *J. Green Build.*, vol. 12, no. 4, pp. 1–20, 2017, doi: 10.3992/1943-4618.12.4.1.
[4] C. Peng;, L. Huang;, and B. Wan, "Novel integrated design strategies for net-zero-energy solar buildings (NZESBS) in Nanjing, China," *J. Green Build.*, vol. 10, no. 3, pp. 89–115, 2015.

[5] Y. L. He, P. Chu, W. Q. Tao, Y. W. Zhang, and T. Xie, "Analysis of heat transfer and pressure drop for fin-and-tube heat exchangers with rectangular winglet-type vortex generators," *Appl. Therm. Eng.*, vol. 61, no. 2, pp. 770–783, 2013, doi: 10.1016/j.applthermaleng.2012.02.040.
[6] L. Chai and S. A. Tassou, "A review of airside heat transfer augmentation with vortex generators on heat transfer surface," *Energies*, vol. 11, p. 2737, 2018, doi: 10.3390/en11102737.
[7] H. Wu, D. S.-K. Ting, and S. Ray, "The effect of delta winglet attack angle on the heat transfer performance of a flat surface," *Int. J. Heat Mass Transf.*, vol. 120, pp. 117–126, 2018, doi: 10.1016/j.ijheatmasstransfer.2017.12.030.
[8] F. A. S. da Silva, D. J. Dezan, A. V. Pantaleão, and L. O. Salviano, "Longitudinal vortex generator applied to heat transfer enhancement of a flat plate solar water heater," *Appl. Therm. Eng.*, vol. 158, no. April, p. 113790, 2019, doi: 10.1016/j.applthermaleng.2019.113790.
[9] Z. Sun, K. Zhang, W. Li, Q. Chen, and N. Zheng, "Investigations of the turbulent thermal-hydraulic performance in circular heat exchanger tubes with multiple rectangular winglet vortex generators," *Appl. Therm. Eng.*, vol. 168, p. 114838, 2020, doi: 10.1016/j.applthermaleng.2019.114838.
[10] Y. X. Li, X. Wang, J. Zhang, L. Zhang, and J. H. Wu, "Comparison and analysis of the arrangement of delta winglet pair vortex generators in a half coiled jacket for heat transfer enhancement," *Int. J. Heat Mass Transf.*, vol. 129, pp. 287–298, 2019, doi: 10.1016/j.ijheatmasstransfer.2018.09.109.
[11] W. Hu, L. Wang, Y. Guan, and W. Hu, "The effect of shape of winglet vortex generator on the thermal–hydrodynamic performance of a circular tube bank fin heat exchanger," *Heat Mass Transf. und Stoffuebertragung*, vol. 53, no. 9, pp. 2961–2973, 2017, doi: 10.1007/s00231-017-2042-3.
[12] L. Zhang, H. Guo, J. Wu, and W. Du, "Compound heat transfer enhancement for shell side of double-pipe heat exchanger by helical fins and vortex generators," *Heat Mass Transf. und Stoffuebertragung*, vol. 48, no. 7, pp. 1113–1124, 2012, doi: 10.1007/s00231-011-0959-5.
[13] C. Zhai, M. D. Islam, R. Simmons, and I. Barsoum, "Heat transfer augmentation in a circular tube with delta winglet vortex generator pairs," *Int. J. Therm. Sci.*, vol. 140, no. March, pp. 480–490, 2019, doi: 10.1016/j.ijthermalsci.2019.03.020.
[14] S. Pourhedayat, S. M. Pesteei, H. E. Ghalinghie, M. Hashemian, and M. A. Ashraf, "Thermal-exergetic behavior of triangular vortex generators through the cylindrical tubes," *Int. J. Heat Mass Transf.*, vol. 151, 2020, doi: 10.1016/j.ijheatmasstransfer.2020.119406.
[15] K. Song and L. Wang, "Effects of longitudinal vortex interaction on periodically developed flow and heat transfer of fin-and-tube heat exchanger," *Int. J. Therm. Sci.*, vol. 109, pp. 206–216, 2016, doi: 10.1016/j.ijthermalsci.2016.06.011.
[16] K. W. Song and T. Tagawa, "The optimal arrangement of vortex generators for best heat transfer enhancement in flat-tube-fin heat exchanger," *Int. J. Therm. Sci.*, vol. 132, pp. 355–367, 2018, doi: 10.1016/j.ijthermalsci.2018.06.011.
[17] A. Kondjoyan and J. D. Daudin, "Effects of free stream turbulence intensity on heat and mass transfers at the surface of a circular cylinder and an elliptical cylinder, axis ratio 4," *Int. J. Heat Mass Transf.*, vol. 38, no. 10, pp. 1735–1749, 1995, doi: 10.1016/0017-9310(94)00338-V.
[18] G. Melina, P. J. K. Bruce, J. Nedić, S. Tavoularis, and J. C. Vassilicos, "Heat transfer from a flat plate in inhomogeneous regions of grid-generated turbulence," *Int. J. Heat Mass Transf.*, vol. 123, pp. 1068–1086, 2018, doi: 10.1016/j.ijheatmasstransfer.2018.03.019.
[19] D. S.-K. Ting, *Basics of engineering turbulence*. Academic Press, New York, 2016.
[20] D. Bradley, M. Lawes, and M. S. Mansour, "Correlation of turbulent burning velocities of ethanol-air, measured in a fan-stirred bomb up to 1.2MPa," *Combust. Flame*, vol. 158, no. 1, pp. 123–138, 2011, doi: 10.1016/j.combustflame.2010.08.001.
[21] D. Bradley, M. Shehata, M. Lawes, and P. Ahmed, "Flame extinctions: Critical stretch rates and sizes," *Combust. Flame*, vol. 212, pp. 459–468, 2020, doi: 10.1016/j.combustflame.2019.11.013.
[22] "Thermal Conductivity of common Materials and Gases." [Online]. Available: https://www.engineeringtoolbox.com/thermal-conductivity-d_429.html. [Accessed: 26-Aug-2020].
[23] "Emissivity Coefficients Materials." [Online]. Available: https://www.engineeringtoolbox.com/emissivity-coefficients-d_447.html. [Accessed: 26-Aug-2020].
[24] G. I. Taylor, "The spectrum of turbulence," *Proc. R. Soc.*, vol. 164, pp. 476–490, 1938, doi: 10.1098/rspa.1927.0039.

[25] "Radiation Heat Transfer." [Online]. Available: https://www.engineeringtoolbox.com/radiation-heat-transfer-d_431.html. [Accessed: 04-Apr-2019].
[26] Promode R. Bandyopadhyay, D. J. Stead, and R. L. Ash, "Organized nature of a turbulent trailing vortex," *AIAA J.*, vol. 29, pp. 1627–1633, 1991.
[27] L. Luo, F. Wen, L. Wang, B. Sundén, and S. Wang, "On the solar receiver thermal enhancement by using the dimple combined with delta winglet vortex generator," *Appl. Therm. Eng.*, vol. 111, pp. 586–598, 2017, doi: 10.1016/j.applthermaleng.2016.09.096.
[28] M. T. Baissi, A. Brima, K. Aoues, R. Khanniche, and N. Moummi, "Thermal behavior in a solar air heater channel roughened with delta-shaped vortex generators," *Appl. Therm. Eng.*, vol. 165, no. March 2019, 2020, doi: 10.1016/j.applthermaleng.2019.03.134.
[29] R. S. Figliola and D. E. Beasley, *Theory and design for mechanical measurements, Fourth edition*. Wiley, New York, 2006.
[30] S. Yavuzkurt, "A Guide to Uncertainty Analysis of Hot-Wire Data," *J. Fluids Eng.*, vol. 106, no. 2, p. 181, 2009, doi: 10.1115/1.3243096.

APPENDIX

Uncertainty

The uncertainty in the experiment is consisted of bias and precision, which could be expressed as [29],

$$E = \sqrt{\text{Bias}^2 + \text{Precision}^2} \tag{12}$$

And the precision in this study was deduced by a 10-times repeating measurement, following the Student's t distribution of 95% confidence interval. Then, the uncertainty of the dependent parameter, $y = f(x_1,x_1,\ldots x_n)$, could be deduced based on the propagation rule [29],

$$E(y) = \sqrt{\sum_{i=1}^{n}\left[\frac{\partial y}{\partial x_i}E(x_i)\right]^2} \tag{13}$$

According to calibration error [30] and the Equation (12) and (13), the uncertainties in this study were estimated and summarized in Table 7.

TABLE 7. Uncertainties of parameters in the experiment.

Parameter	$\bar{U}$	$\bar{V}$	$\bar{W}$	Nu/Nu_0
Uncertainty	0.14 ms^{-1}	0.05 ms^{-1}	0.03 ms^{-1}	0.066
Parameter	λ	λ	σ_s	
Uncertainty	0.02 ms^{-1}	0.10 mm	23 s^{-1}	